Hydrogel matrices based on elastin and alginate for tissue engineering applications

DOI:
10.1016/j.ijbiomac.2018.03.091

Document Version
Accepted author manuscript

Hydrogel matrices based on elastin and alginate for tissue engineering applications

Raquel Silva[1], Raminder Singh[2,3], Bapi Sarker[1], Dimitrios G. Papageorgiou[4,5], Judith A. Juhasz-Bortuzzo[1], Judith A. Roether[6], Iwona Cicha[2], Joachim Kaschta[6], Dirk W. Schubert[6], Konstantinos Chrissafis[4], Rainer Detsch[1], and Aldo R. Boccaccini[1*]

[1] Institute of Biomaterials, Department of Materials Science and Engineering, University of Erlangen-Nuremberg, 91058 Erlangen, Germany

[2] Cardiovascular Nanomedicine Unit, Section of Experimental Oncology and Nanomedicine, ENT Department, University Hospital Erlangen, 91054 Erlangen, Germany

[3] Laboratory of Molecular Cardiology, Medical Clinic 2, University Hospital Erlangen, 91054 Erlangen, Germany

[4] Solid State Physics Section, Physics Department, Aristotle University of Thessaloniki, 541 24 Thessaloniki, Greece

[5] School of Materials and National Graphene Institute, University of Manchester, Oxford Road, M13 9PL Manchester, United Kingdom.

[6] Institute for Polymer Materials, Department of Materials Science and Engineering, University of Erlangen-Nuremberg, 91058 Erlangen, Germany

*Corresponding author: Aldo R. Boccaccini and Raquel Silva

e-mail: aldo.boccaccini@ww.uni-erlangen.de

University of Erlangen-Nuremberg

Institute of Biomaterials, Department of Materials Science and Engineering

91058 Erlangen, Germany, Tel: +49(0)9131 85-28601

Abstract

Hydrogels from natural polymers are widely used in tissue engineering due to their unique properties, especially when regarding the cell environment and their morphological similarity to the extracellular matrix (ECM) of native tissues. In this study, we describe the production and characterization of novel hybrid hydrogels composed of alginate blended with elastin from bovine neck ligament. The properties of elastin as a component of the native ECM were combined with the excellent chemical and mechanical stability as well as biocompatibility of alginate to produce two hybrid hydrogels geometries, namely 2D films obtained using sonication treatment and 3D microcapsules produced by

pressure-driven extrusion. The resulting blend hydrogels were submitted to an extensive physico-chemical characterization. Furthermore, the biological compatibility of these materials was assessed using normal human dermal fibroblasts, indicating the suitability of this blend for soft tissue engineering.

Keywords: alginate, elastin, hybrid hydrogels, soft matrices, tissue engineering.

1. Introduction

Tissue engineering offers the potential to create functional and viable tissue constructs for patients requiring organ replacement [1]. These constructs can be cultivated *in vitro* and then transplanted into the patient or they can be created *in vivo* by implanting a scaffold into the patient´s body allowing cellular infiltration. Living cells are the key players in tissue engineering, based on their ability not only to produce the native extracellular matrix (ECM), but also to self-organize into complex tissues on the condition that their native biochemical and biophysical microenvironment can be recapitulated [2]. Matrices for tissue engineering should therefore serve as templates to guide cell growth and tissue development. Due to the fact that cells display different phenotypes depending on their microenvironment, the biochemical and the biophysical properties of the matrices greatly influence the functional tissue regeneration process [2]. Although different biomaterials have been proposed for tissue engineering, hydrogels remain attractive candidates due to their structural similarity to the native ECM, inherent biocompatibility, tuneable viscoelasticity, high water content and high permeability for oxygen and essential nutrients [3,4]. The native ECM can well be viewed as a hybrid hydrogel containing multiple structural and functional components interdigitated at all length scales [5–9]. Thus far, several materials have been utilized for different tissue engineering applications, including reconstituted ECM components or natural proteins, carbohydrates and synthetic hydrogels [2]. Alginate, an anionic biopolymer consisting of linear chains of α-L-glucuronic acid and β-D-mannuronic acid, is a particularly suitable material to prepare hydrogels due to its favourable properties in terms of biocompatibility, biodegradability, non-antigenicity and chelating ability [10,11]. The methods of alginate hydrogel preparation are usually selected with the aim to control the gelification phenomenon, which

leads to desired size ranges depending on various factors including alginate concentration/viscosity, counter-ion concentration and the rate of adding counter-ion solution onto the alginate solution, among others [12]. However, alginate does not promote cell attachment, resulting in poor cell-material interactions, and is furthermore characterized by slow degradation and unfavourable degradation kinetics [13–15]. Therefore, the use of hybrid materials composed of a polysaccharide and proteins represents a promising approach expected to improve hydrogel biocompatibility. In particular, natural proteins that show similarity to those in the ECM are excellent candidates to enhance cellular interactions of alginate and to tailor the degradability of the hydrogels for soft tissue regeneration [16–18].

Natural proteins exhibit distinct primary, secondary and tertiary structures that determine their main function. Furthermore, they can provide structural support for cells, and stimulate active cellular responsiveness, biological recognition, and cell-triggered remodelling [9]. Elastin is one of the major proteins present in the native ECM has the particularity to provide elasticity to tissues and organs. Elastin is synthesized by a variety of cells including smooth muscle cells, endothelial cells, fibroblasts and chondrocytes. This structural protein is the essential component of the elastic fibres that provide elasticity to different tissues, such as blood vessels, skin, bladder, lungs and vocal folds [19]. Elastin is a protein comprised of approximately 800 amino acid residues [20,21]. It is synthesized from a ≈72 kDa precursor, tropoelastin, that is water soluble, non-glycosylated and highly hydrophobic and can be further converted into insoluble elastin polymer [22–24]. In general, the tropoelastin molecule consists of two types of domains: hydrophobic domains rich in nonpolar amino acids (glycine, valine, alanine and proline residues, which often occur in repeats of tetra-, penta- and hexapeptides), and hydrophilic domains (mainly lysine and alanine residues, which are potentially involved in crosslinking domains of tropoelastin) [25]. Due to its highly crosslinked nature, elastin has very poor solubility and is difficult to process into new biomaterials. As a consequence, soluble forms of elastin including tropoelastin [1,26], α-elastin [27–30] and elastin-like polypeptides [21,31–33] are frequently used to develop elastin-based biomaterials and crosslinking is normally required to produce stable hydrogels.

In our previous published work we successfully obtained new blends between alginate and keratin protein. Keratin is distinct from elastin by the high content of cysteine (9%) residues responsible for the formation of disulfide bonds, which gives high strength to keratin materials. One the other hand, elastin is mainly composed of glycine (32%), alanine (24%), proline (12%) and valine (11%) that characterize the hydrophobic regions of elastin in the human body. Keratin materials present high mechanical strength, and on the other hand soluble elastin enhances elastin synthesis *in vivo*. Therefore, the aim of our study was to combine bovine elastin, known for its excellent biological properties, with alginate, which can form hydrogels, in order to achieve hydrogel matrices without the use of crosslinking agents. We applied two different technologies, namely i) sonication treatment to prepare 2D matrices and ii) pressure driven extrusion technique to obtain 3D hydrogel-structures. Following an extensive physico-chemical characterization of both geometries, cell biology studies using normal human dermal fibroblasts were performed whereby cells were seeded onto prefabricated porous films (2D) to assess cell-material interactions.

2. Experimental Section

2.1. Materials

Sodium alginate (sodium salt of alginic acid from brown algae, suitable for immobilization of micro-organisms, MW 100,000-200,000 g/mol, guluronic acid content 65-70 %) was acquired from Sigma-Aldrich, Germany, as well as the soluble elastin from bovine neck ligament. Calcium chloride di-hydrate ($CaCl_2$ x $2H_2O$) was purchased from VWR International, Belgium. All other reagents were analytical grade and purchased from Sigma-Aldrich, Germany.

2.2. Preparation of blend solutions

Elastin solution was prepared by dissolving the elastin powder in distilled water. Alginate (2%) and elastin (1%) were mixed to prepare blends. For that purpose, the alginate solution (2%; w/v) was previously heated to 37 ºC to improve handling by pipetting, and was added to the prepared protein solution (1%; w/v). The blend solution of alginate/elastin (Alg/E) and only alginate solution (Alg) were further submitted to an ultrasound treatment to produce hydrogel films

(2D) and to a pressure-driven extrusion technique in order to prepare microcapsules (3D), as described in detail below.

2.3. Sonochemical preparation of 2D hydrogels

The experimental set-up used was composed of a probe type ultrasound source (20 kHz Sonics & Materials Vibracell CV 33) fitted with a 3 mm diameter titanium micro-tip. The power delivery was controlled as percentage amplitude. The reaction vessel, containing 14 mL of blend solution (open glass cell with 19 mm of diameter and 75 mm of height), was a similar device as previously described [34]. The sonication treatment was carried out for 3 min and monitored in 58 s increments. A pulsed duty cycle of “8 s on, 2 s off“ was used. The blend solution (14 mL) was transferred into a 10 cm glass Petri dish (VWR, Germany) and left at 37 ºC for approximately 30 min to dry. Calcium chloride solution (0.1 M) was poured on the formed hydrogel-films and left for 15 min to allow ionic gelation. Afterwards, films were washed three times with ultrapure water (Direct Q®, Merck Milli-Pore, Germany), or with cell culture medium and discs of 13.5 mm in diameter were punched out using a stainless steel cutter.

2.4. Pressure-driven extrusion preparation of 3D hydrogels

Microcapsules were produced according to the previously published method [18] by applying the pressure-driven extrusion technique. In brief, Alg (2%; w/v) and the blend solution of Alg/E (2% and 1% w/v, respectively) were transferred into an extrusion cartridge (Nordson EFD, USA) connected to a high precision fluid dispenser (Ultimus V, Nordson EFD, USA). Microcapsules obtained by applying different air pressures (0.55 bar to 2.5 bars) were collected in a beaker containing calcium chloride solution (0.1 M) and kept for 10 min to allow ionic gelation. A further washing procedure was performed three times with water in order to remove adherent calcium chloride, and to form microcapsules in the size range of 700-800 µm.

2.5. Physico-chemical characterization of hybrid hydrogels

2.5.1. Fourier Transform Infrared Spectroscopy (FTIR)

The chemical structure of the samples was assessed by Fourier transform infrared (FTIR) spectrometer (Nicolet 6700, Thermo Scientific, USA). The

previously dried hydrogels were used to record attenuated total reflectance Fourier transform infrared (ATR-FTIR) spectra of 2D hydrogels of Alg and Alg/E. The pure elastin sample was also analysed.

2.5.2. Thermogravimetric analysis

Thermogravimetric analysis was carried out with a SETARAM SETSYS TG/DTA 16/18 instrument. Samples were placed in alumina crucibles and an empty alumina crucible was used as reference. Alg and Alg/E, 2D and 3D dried hydrogel samples, were heated from ambient temperature to 800 °C in a 50 mL min^{-1} flow of dry air at a heating rate of 10 °C min^{-1}. Continuous recordings of sample temperature, weight and heat flow were taken.

2.5.3. Water uptake

The water uptake behaviour of the 2D and 3D hydrogels were evaluated at pH 7.4 and 37 °C in two different solvent environments: Dulbecco's modified eagle medium (DMEM, Gibco, Germany) and Hanks' balanced salt solution (HBSS, Sigma Aldrich, Germany).

All hydrogel samples were dried using a critical point dryer (Leica EM CPD300, Germany) prior to use and were weighted dry. The samples were then swelled in 2 mL of solvent. The swelling patterns of matrices were followed over a period of 3 days at several intervals. After each time period, the specimens were withdrawn from the aqueous medium and the excess of surface liquid was removed gently with a wiping paper (Whatman Pergamyn Paper), then the weight was recorded using an analytical balance (Scaltec, Germany). The specimens were again returned to the different media after weighting. The water uptake was calculated by using the following equation (1), where W_w and W_d are the weights of swollen and dried hydrogels, respectively:

$$\text{Water uptake}(\%) = \frac{(W_w - W_d)}{W_d} \times 100 \quad (1)$$

Each experiment was repeated five times and the average was considered to be the representative water uptake value for the sample (± standard deviation).

2.5.4. Weight loss

Degradation of 2D and 3D hydrogels was evaluated through their immersion in HBSS and DMEM at 37°C for a period of up to 21 days. The weight of the hydrogel samples was measured after the drying process in a critical point dryer, before and after incubation in different solvents. The percentage of weight loss was calculated according to the equation (2), where W_i and W_d correspond to the initial weight and dried sample weight, respectively:

$$\text{Weight loss}(\%) = \frac{(W_i - W_d)}{W_i} \times 100 \quad (2)$$

At least five specimens were tested for each type of hydrogel, and the average value was considered to be the weight loss value (± standard deviation).

2.5.5. Protein quantification

The 2D and 3D hydrogels were immersed in 2 mL of HBSS and serum free DMEM (Gibco), respectively, at 37 °C and pH 7.4. At selected times, the solution was removed and collected for protein release analysis, and 2 mL fresh media was added. The elastin concentration in the released buffer was determined by the colorimetric Lowry method [35], using bovine serum albumin as a standard. The absorbance was measured at 750 nm, using a UV-Vis spectrophotometer (Specord 40, analytik Jena, Germany). The percentage of protein released from the hybrid hydrogels was calculated by using equation 3, as follows:

$$\text{Protein released}(\%) = \frac{[C]_f}{[C]_i} \times 100 \quad (3)$$

where, $[C]_i$ is the initial protein concentration and $[C]_f$ is the protein concentration measured in the supernatant.

Measurements were recorded in triplicate and the results were expressed as mean value ± standard deviation.

To study the degradation mechanism of low molecular weight compounds in polymers and hydrogels a simple power law equation can be applied (Ritger-Peppas equation [36]):

$$M_t/M_\infty = kt^n \quad (4)$$

M_t/M_∞ is the fractional protein release at time t; t is the release time; k is the kinetic constant that measures the protein release rate, and n is the diffusion exponent that depends on the release mechanism and the geometry of the matrix. To determine n values, Eq. (4) is modified in Eq. (5) and n is obtained from the slope of the plot of log (%released) vs. log t.

$$\log(\%\text{released}) = \log(M_t/M_\infty) = \log k + n \log t \quad (5)$$

2.5.6. Scanning electron microscopy (SEM)

The morphological analysis of the 2D and 3D hydrogels was performed using scanning electron microscopy (SEM). The samples for SEM analysis were dried with a critical point dryer. 2D hydrogel samples were analysed using an AURIGA-Zeiss SEM and in the case of 3D hydrogels, they were visualized using a LEO 435 VP SEM (LEO Electron Microscopy Ltd, Cambridge, UK).

2.6. Mechanical characterization

Mechanical properties of the 2D hydrogels were determined with a dynamic mechanic thermal analyser (DMTA, Rheometric Scientific). The measurements were performed in compression at 25 °C, in a dynamic frequency sweep (0.1 Hz to 25 Hz), at which a sinusoidal deformation of constant amplitude was applied on the cylindrical samples (16 mm of diameter). All measurements were carried out in the linear viscoelastic regime with a strain of 0.1 %. During the period of the measurement it was proven that no change in material properties occurred due to evaporation of water. Measurements were recorded in quadruplicate and the results were expressed as mean value ± standard deviation.

2.7. Cell-material interaction using normal human dermal fibroblast cells

2.7.1. Cell culture

Normal human dermal fibroblasts (PromoCell, Germany) were cultured in DMEM supplemented with 10% (v/v) FCS and 1% (v/v) antibiotic-antimycotic, at 37 °C, in a controlled atmosphere of 5% CO_2 and 95% relative humidity. A

monolayer of fibroblasts in their growth phase (≈ 90% confluence) was harvested using trypsin/ EDTA (0.05%) (Life Technologies, Germany). Cells were counted using trypan blue exclusion method (Sigma-Aldrich, Germany) before seeding on hydrogels.

2.7.2. Cell seeding onto 2D hydrogels

The prepared circular 2D hydrogels composed of Alg and Alg/E were placed into a 24-well plate (VWR Int., Germany) and washed with DMEM. For analysis of cell adhesion, $7.5x10^4$ cells/film were seeded and incubated at 37 °C with 95% relative humidity and 5% CO_2. The culture medium was changed the day after seeding, and then every two days.

2.7.3. Cell staining

To assess the viability of fibroblasts, live staining was performed with calcein acetoxymethyl ester (Calcein AM, Invitrogen™, USA) after 3, 7 or 10 days of cultivation. The nuclei were visualized by blue nucleic acid stain, DAPI (4',6-diamidino-2-phenylindole, dilactate, Invitrogen™, USA) which preferentially binds to A (Adenine) and T (Thymine) regions of DNA. The images of calcein-DAPI stained cells were taken by fluorescence microscope (FM) (Axio Scope A.1, Carl Zeiss Microimaging GmbH, Germany).

2.7.4. Mitochondrial activity

Mitochondrial activity of fibroblasts grown on different 2D hydrogels was assessed through the enzymatic conversion of tetrazolium salt (WST-8 assay kit, Sigma Aldrich, Germany) after 3, 7 or 10 days of cultivation. Culture medium was completely removed from the samples and freshly prepared culture medium was added containing 1 % (v) WST-8 assay kit, followed by incubation for 2 h. Subsequently, 100 µL of supernatant from each sample was transferred into a well of a 96 well-plate and the absorbance was measured at 450 nm with a microplate reader (SpectraMax® Plus, Molecular Devices, USA).

2.8. Statistical analyses

Statistical analyses were performed by one-way analysis of variance (ANOVA) on the 2D hydrogels. The pairwise comparison of the means was performed

with the Bonferroni's test (post hoc comparison), where p-values < 0.05 were considered statistically significant.

3. Results and Discussion

3.1. Physico-chemical characterization of 2D and 3D hydrogels

3.1.1. Chemical composition: ATR-FTIR assessments

FTIR is a useful technique to evaluate the chemical composition of blend materials and, in the case of proteins, can be used to determine the protein conformation. **Figure 1** shows the representative infrared (IR) absorption spectra of the materials, which characterize pure elastin, Alg and the blend Alg/E 2D hydrogels. The FTIR spectra of Alg has been widely reported in the literature and is characterized by the peaks which fall at around 3447, 1615, 1421, and 1035 cm^{-1} and are attributed to the stretching of O-H, -COO (asymmetric), $-COO^-$ (symmetric), and C-O-C, respectively [37].

The main features observed in the FTIR spectra of proteins are those associated with the planar peptidic bond vibrational modes, the amide bands. Their positions, widths and intensities are characteristic of the associated vibrational modes and thus of the local geometry of the peptidic chain. They are the amide I (1700-1600 cm^{-1}, C=O stretching), amide II (1600-1500 cm^{-1} NH bending and C-H stretching vibration), and amide III from 1350 to 1200 cm^{-1} (combination of C-N stretching and C=O bending vibration) [38]. Of all the amide modes of the peptide group, the single most widely used one in studies of protein secondary structure is the amide I. This vibrational mode originates from the C-O stretching vibration of the amide group (coupled to the in-phase bending of the N-H bond and the stretching of the C-N bond), and gives rise to IR band(s) in the region between approximately 1600 and 1700 cm^{-1} [39,40]. A critical step in the interpretation of IR of proteins is the assignment of the amide I component bands to different types of secondary structure [41]. The positions of these bands indicate the conformations of the proteins: 1650 cm^{-1} (random coil) and 1630 cm^{-1} (β- sheet) for amide I; 1540 cm^{-1} (random coil) and 1520 cm^{-1} (β-sheet) for amide II; 1230 cm^{-1} (random coil) and 1270 cm^{-1} (β-sheet) for amide III [42,43]. The IR spectra of elastin showed a peak at

1657 cm^{-1} for amide I, 1540 cm^{-1} for amide II, and 1236 cm^{-1} for amide III, assigned to random coil-conformation [44,45].

The blend with Alg presents a shift in IR absorbance to lower wavenumber upon formation of hydrogels. A strong absorbance signal at 1620 cm^{-1} in the amide I, together with a strong shoulder at 1533 cm^{-1} and a shift to higher wavenumber of the amide III at 1290 cm^{-1}, indicates that the use of mechanical treatment, such as sonication, induces a structural change into a more β-sheet conformation in elastin. As reported for other fibrous proteins, the presence of the β-sheet structure plays an important role in the hydrogel network formation. The mechanism of gelation is the self-assembly of the protein chains into physically crosslinked β-sheet crystals. Exposure to heat, physical shear, or to some organic solvents can induce the formation of insoluble crystallized structures [46–48]. In this study, 2D hydrogels were achieved in two main steps. Firstly, the solutions were submitted to an ultrasound treatment to induce the sol-gel process. Sonication treatment produces mechanical vibration causing the formation and collapse of bubbles, leading to cavitation, where extreme local effects (heating, high pressure, high strain rates [49–51]) occur, inducing the production of radicals such as hydroxyl ($^{\bullet}OH$) and hydrogen ($H^{\bullet}$) radicals, and in the presence of oxygen (O_2), superoxide ($O_2^{\bullet-}$) and hydroperoxyl radicals ($HO_2^{\bullet}$) [52–54]. Therefore, sonication can lead to a change in the protein conformation, enhancing electrostatic interactions and promoting changes in hydrophobic hydration. As a consequence, the molecular chains could become closer, thus stabilizing the supramolecular β-sheet structure of elastin. The gelation process is finalized with the addition of calcium chloride solution, where the Ca^{2+} ions can neutralize electrostatic repulsions and form salt bridges between protein aggregates and between Alg molecules. This behaviour can also be inferred from the IR spectra of Alg/E, being possible to detect the main peaks of elastin and Alg (**Fig. 1**).

(Figure 1)

3.1.2. Thermogravimetric analysis (TGA)

To assess the thermal degradation of the Alg and Alg/E 2D hydrogels TGA was performed. **Figure 2** shows the weight percentage change during heating and

also the first derivate of the weight percentage function which reveal the degradation rate of each component in the Alg/E hydrogels.

The thermograms of Alg and Alg/E demonstrated that these two different materials exhibit quite similar thermal behaviour. Alg undergoes four degradation steps. The first stage (between 30-170 °C) is related to the evaporation of water and corresponds to the dehydration of the sample. The second stage (205-320°C) refers to the decomposition of Alg by the dehydration of the saccharide rings, breaking up of C-H bonds and breaking of the C-O-C glycoside bonds in the main polysaccharide chain. After this step, up to 497 ^{o}C, Na_2CO_3 and a carbonized material are formed. In the third degradation step, from 497 to 520 ^{o}C, the decomposition of the carbonized material is very fast, resulting in Na_2CO_3 [55]. The pure Alg 2D hydrogel loses 20.5 wt. % of its mass during this step. After this sharp step there is a plateau and the final degradation step of Alg is observed above 710 ^{o}C, where Na_2CO_3 decomposes and the sample loses only 4% of its initial mass.

Regarding the hybrid sample, the first and second degradation steps of Alg/E occur at the same temperature intervals observed for Alg, indicating decomposition in a similar manner. The major difference between the two thermograms is observed at the third decomposition step, where a violent combustion takes place. Alg/E blend starts this decomposition step at 487 ^{o}C (10 ^{o}C earlier than for pure Alg) and loses almost 6.2% of its initial mass. In the temperature range from 500 to 670 ^{o}C a plateau is formed in the thermogram of Alg/E films, while above 670 ^{o}C the final degradation step of Alg/E is evident (40 ^{o}C earlier than pure Alg), as indicated also from the wide peak in the DTG graph. The decomposition of sodium carbonate, which has been formed during the heating process at lower temperatures, takes place in this temperature range. Regarding the remaining mass loss percentages, the Alg degraded almost completely and the mass residue was about 9%. Conversely, the Alg/E sample showed a higher percentage of mass residue (almost 15%). Moreover, comparing both samples, it was observed that they presented only slight differences, in the temperature range 30-500 ^{o}C. The specific differences in the mass loss curves, above 500 ^{o}C, could be related to a certain amount of elastin that remained unblended with Alg, which normally presents low molecular weight chains that were unable to form a gel network.

Thermogravimetric analysis was also performed on 3D hydrogels in the same conditions as used for 2D hydrogels. The results from the measurements performed on the 3D hydrogels did not reveal significant differences in the thermal degradation between Alg and Alg/E hydrogels. The trend observed during the degradation process was almost identical for both samples. A small difference was detectable above 400 ^{o}C. From that point, Alg decomposed at slower rates than the hybrid samples, a fact which resulted in higher mass residue of Alg. Compared to the films, microcapsules underwent the same degradation steps, until 450 ^{o}C, at slightly elevated temperatures. However, the most significant difference was that the fast decomposition detected in the films at 485-520 ^{o}C, was not observed in microcapsules, most probably due to different water contents in the different sample geometries. Another difference between 2D and 3D samples worth mentioning is that in in the case of Alg/E hydrogel films the residue is higher than that of Alg samples, while for the 3D samples (capsules) the Alg residue is higher. This can be explained by the fact that for the fabrication of the hydrogel films, ultrasound was used, which can promote and increase the interactions between alginate and elastin, producing a significantly more stable structure.

(Figure 2)

3.1.3. Water uptake

The determination of the amount of water contained in the hydrogels is an important criterion for characterizing the hydrogel for biomedical applications [56]. The water uptake of the hydrogel (often expressed as % of water uptake) is directly proportional to the amount of water imbibed within the hydrogel. The amount of water influences the diffusional properties of a solute through the hydrogel, since the softer material will have the ability to accumulate more water. This is particularly important for implantable materials because this property allows the diffusion and exchange of nutrients and waste through the entire scaffold. Furthermore, it is an important indicator of the surface area for the cells to adhere, which is essential for tissue engineered scaffolds. The water uptake characteristics of hydrogels are generally influenced by many factors, such as gel composition, charge, and crosslink density [57]. However, it must

be noted that an overtly increased water uptake can also negatively affect the properties of a biomaterial (e.g. pore size, diffusion rate, and mechanical property), and therefore a balance should be found [58]. In our study, the water uptake ability of 2D and 3D hydrogels was analysed in different media, namely HBSS and DMEM (**Figure 3)**. The aim of using these different solutions was to investigate whether specific water uptake effects occur upon using a normal medium which mimic the cell environment (e.g. DMEM) in comparison with an isotonic solution such as HBSS.

(Figure 3)

The obtained results indicated that the addition of elastin to prepare 2D and 3D hydrogels led to a small decrease of water uptake, which was independent of the media used (**Figure 3**). These results were confirmed later by the comparison of the mechanical properties between pure Alg and Alg/E hydrogels. The presence of protein can lead to a decrease of network space and, in consequence, reduce the amount of water that enters the hydrogels. However, the differences between the two hydrogel types were small, indicating that the electrostatic and hydrophobic interactions that occur between the protein chains and also with Alg molecules did not create a significant difference in the diffusion of the medium inside the network.

Comparing the 2D and 3D hydrogels, the water uptake was higher for the 3D hydrogels, supporting the results of the thermogravimetric analysis, which showed the high content of water in microcapsules. These two different geometries showed the ability to transport nutrients inside the matrix, presenting no obvious differences upon immersion in different media, which is extremely important for cell encapsulation purposes. Our results thus demonstrated that the presence of elastin in the hybrid hydrogel does not negatively affect the water uptake properties, and that both geometries seem to be promising for tissue engineering.

3.2.4. Degradation studies: Weight loss and protein release

The degradation behaviour of 2D hydrogels was evaluated in terms of weight loss over 21 days in the presence of HBSS and DMEM at 37 °C. However, for

the 3D hydrogels, the weight loss was not possible to be determined due to the loss of microcapsules during the drying process. As shown in **Figure 4,** the weight loss of hybrid hydrogels was lower when compared with Alg. This fact can be related to the sonication treatment as, according to the literature [59], ultrasound induces the degradation of polysaccharides, producing fragments with lower molecular weight that lead to a decreased stability of the formed hydrogels. However, the difference between Alg and Alg/E hydrogels was not significant, likely due to the presence of some elastin molecules with low molecular weight chains that remained unblended with Alg, and were not able to form a gel network [10]. Comparing the two different media, no significant difference in weight loss was observed.

(Figure 4)

In order to better understand the degradation behaviour of the produced matrices, the protein release from 2D and 3D hydrogels was monitored over time. For that purpose, the effect of HBSS and DMEM (pH 7.4, 37 ºC) on the elastin release from 2D and 3D hybrid hydrogels was investigated (**Figure 5**). In both 2D and 3D hydrogels, the release of protein started immediately after 30 min of incubation and decelerated with prolonged incubation time. The observed high initial protein release could be due to the slight instability of the protein network immediately upon rehydration in medium. Interestingly, a comparatively higher amount of elastin was released from Alg/E immersed in DMEM than in HBSS. This phenomenon might be attributed to the presence of calcium salt in HBSS but not in DMEM. Thus, the calcium ions in HBSS are expected to interact with the hydrogels, increasing the stability of both 2D and 3D hydrogels.

Comparing both geometries, the 2D hybrid hydrogels demonstrated lower amount of protein released over time. This lower amount of elastin released from 2D geometries as compared to 3D hydrogels indicated that a significant quantity of elastin remained in the material that could enhance cell-material interactions. However, it is possible to increase the stability of these materials by a covalent crosslinking between Alg and E. Previous results, from our research group, demonstrated that the chemical modification of alginate leads

to an improvement of the stability of the material in physiological-like conditions. Alginate di-aldehyde (ADA) is a partially oxidized product of alginate which facilitates the covalent crosslinking with the protein through Schiff's base formation due to the reaction of free amino groups of protein and available aldehyde groups of ADA. In this way the biodegradability of the alginate-protein crosslinked hydrogel can be tuned by using ADA of different degrees of oxidation which can control the hydrolysis properties of alginate and also by changing the composition of ADA and the protein [18].

(Figure 5)

To determine the release mechanism, the experimental data were fitted to the semi-empirical power law model [60] given by the Ritger–Peppas equation (Eq. (4)). This equation is further modified to determine the diffusional exponent n (Eq. (5)), which depends on the release mechanism and the geometry of the matrix [36,60]. There are three different mechanisms that can be concluded from the n value. The release from a thin film geometry like the 2D hydrogels follows a purely Fickian diffusion law when $n = 0.5$. For $0.5 < n < 1.0$, anomalous (non-Fickian) transport is present and for $n = 1.0$, the release is dominated by Case II transport (matrix relaxation or swelling-controlled mechanism). In the case of spherical samples such as our 3D hydrogels, the diffusion is purely Fickian when $n = 0.43$. For $0.43 < n < 0.85$, anomalous (non-Fickian) transport is present and for $n = 0.85$, the release is dominated by Case II transport (matrix relaxation or swelling-controlled mechanism).

The results presented in Table 1 indicate that when the 2D hydrogel samples were immersed in HBSS and DMEM, the release of protein was dominated by anomalous transport (non-Fickian), because n values are higher than 0.5. This is an indication of the superposition of both extreme phenomena: protein diffusion and macromolecular chain relaxation/degradation. In the case of the release rate, k, there were no significant differences between HBSS and DMEM media.

For 3D hydrogels, the release mechanism was dominated by Fickian diffusion, e.g. it involves predominantly the diffusion of elastin. The values of release rate, k, were higher in DMEM as compared with HBSS media. This indicates that the

DMEM improves the release of protein from the hydrogels, probably due to the increase in degradation rate.

The release results thus clearly support the notion that the protein release from the hydrogels is affected by its geometry and, in the case of capsules, also by the medium. The high correlation coefficient "R^2" (above 0.95) further supports the validity of these results.

(**Table 1**)

3.2.5. SEM analysis

Biomaterials for tissue engineering should possess porous structure to improve the transport of nutrients and oxygen into and out of the matrix. However, as the morphology of the pores also affects the degradation kinetics and the mechanical properties, a compromise should be found to achieve a stable and functional biomaterial. Therefore, the morphological study was carried out in order to analyze the 2D and 3D produced matrices. In the case of 2D hydrogel, the morphology of Alg/E samples was analyzed in cross-section (**Figure 6)**. SEM images of Alg (Fig. 6a) were presented in a previous publication [61]. The SEM images demonstrated that Alg/E 2D formulations exhibit almost the same structure as pure alginate, however no quantitative microstructural analysis was carried out. At the same time, this morphology can explain the results of the water uptake studies, where the differences between Alg and Alg/E were negligible.

Regarding the morphology of the 3D hydrogels, it was observed that Alg microcapsules exhibit a folded surface structure in regular configurations (**Figure 7**). The results demonstrated that the blend with elastin led to a less folded, smoother surface, indicating a more homogeneous material. The differences of sizes of the microcapsules can be explained by the fact that in the hybrid solutions, the macromolecules of E and Alg can interact through hydrogen bonds, carboxylic groups and van der Waals forces which can lead to the formation of microcapsules with large sizes when compared with microcapsules prepared only with alginate.

(Figure 6)

(Figure 7)

3.3. Mechanical properties

The mechanical and viscoelastic properties of 2D hydrogels were evaluated by dynamical mechanical thermal analysis (DMTA), an adequate non-destructive tool for characterizing biomaterials. Regarding the degradation and its influence on the mechanical properties of the materials, it must be considered that DMTA applies a stress on the hydrogel sample, which can influence the gel composition and mechanical stability. All DMTA measurements were carried out over a frequency range of 0.1 to 10 Hz, which covers the characteristic timescales of periodic loads that occur in the body. This range matches for example the frequency of skeletal movement or the passage of blood [62]. In order to mimic the cell environment, these experiments were carried out upon immersion in DMEM. **Figure 8** shows the results obtained by frequency scans from the hydrogel samples that were immersed in DMEM over 21 days. The storage modulus (E') is related to the amount of energy stored by the material during a cycle. An increase in E' with the increase of frequency was verified for all samples. The data in Figure 8 show that the blend with elastin promoted an increase in E' from ≈100 to ≈220 kPa (evaluated to 10 Hz). The results further demonstrated that the elastic moduli of the blend were similar to those found in native elastin [19]. This result is consistent with the water uptake ability of the Alg and the plasticization effect of water molecules in polysaccharides, which increases the molecular mobility, concomitantly decreasing the stiffness of the matrix [63]. The measurements performed over time demonstrated that the storage modulus values decreased after 3 days of incubation. This result can indicate not only the degradation of the material, but also the presence of free elastin molecules, which were not completely blended with Alg and were released after 3 days of immersion, leading to the reduction in storage modulus.

The damping properties of the materials were also analysed by monitoring the variation of tan δ with frequency, as depicted in Figure 8. The loss factor (tan δ), is the quotient of viscous modulus (E''), related to the mechanical energy lost by viscous mechanisms, to the elastic modulus (E'), which is proportional to the energy stored in the elastic component [64]. Furthermore, tan δ gives

information whether the given material is solid with perfect elasticity (tan δ = 0), liquid with pure viscosity (tan δ= ∞), or shows viscoelastic properties (0<tan δ < ∞). Our data showed that tan δ tended to decrease with the increase in frequency, indicating that the materials became more elastic. Furthermore, within the uncertainty, tan δ was constant for Alg. For Alg/E, tan δ was constant at high frequencies (higher gel behaviour), but increased at lower frequencies. This indicates an additional relaxation process due to the presence of elastin. Moreover, as shown in Figure 8, Alg hydrogel exhibited values of tan δ higher than Alg/E, indicating that this material possesses higher capacity to dissipate energy. Over time, the tan δ values of the Alg samples did not exhibit significant variation, suggesting that the damping properties were not dependent on time. However, the presence of elastin resulted in an increase of tan δ values after 21 days, which indicates that the hybrid hydrogels dissipate more energy over the storage time.

(**Figure 8**)

The storage modulus can furthermore provide information about the change in viscoelastic properties and the degree of crosslinking. The storage modulus E' increases with increasing frequency (υ), according to a power law with the exponent n. E'_0 is the storage modulus at a frequency of zero.

$$E' = K\nu^n \quad (4)$$

The exponent n of the power law is shown as the slope of the fitting curves of the storage modulus. The power law exponent reflects the viscoelastic properties of the material as it describes its change with frequency (**Figure 9**). Lower values of n indicate a smaller frequency dependence and therefore a more elastic behaviour for which n=0. In the case of Alg, the slope of the fitting curve decreased after 3 days and it was nearly constant over time until 21 days. In accordance with these results, a decrease in viscoelastic properties of Alg hydrogels was observed after 3 days in DMEM. However, Alg/E hydrogels exhibited stability of their viscoelastic properties over time, reaching a plateau after 7 days of incubation.

(**Figure 9**)

Further information on the material behaviour can be obtained by plotting the intercept of the fitting curve of the logarithmic storage modulus. The storage modulus E' is related to crosslink density n_c (number of crosslinks per unit volume) according to the equation:

$$E' \sim 3n_c T \quad (5)$$

Comparing both types of 2D hydrogels, we concluded that the blend with elastin led to a higher degree of crosslinking, thus being a more robust matrix. The mechanical tests can therefore provide important information to tune the physico-chemical properties of the materials for further applications in tissue engineering.

3.4. Cell-material interaction

One of the most important functions of tissue engineered matrices is to provide a framework and initial support for the cells to attach and proliferate [65]. The biological performance of biomaterials *in vitro* must be characterized in order to evaluate their suitability for their potential use in humans. Therefore, it is important to test the cell-material interaction *in vitro* prior to *in vivo* applications. In this study, we have used human fibroblasts, which are the most abundant cells in various tissues and play an important role in physiological processes such as wound healing, angiogenesis and tissue regeneration. Fibroblasts secrete growth and angiogenic factors, i.e. fibronectin, transforming growth factor (TGF-β1), basic fibroblast growth factor (bFGF), collagen I and III, connective tissue growth factor, etc., and this feature makes them the key players in the control of the extracellular environment, as well as in the regulation of the neighbouring cell behaviour and their response to the environment [66–69]. To investigate whether the cell-material interactions are improved by the presence of elastin in the hydrogel, the attachment and growth, as well as cell morphology and mitochondrial activity of primary fibroblasts were analyzed and compared for Alg and Alg/E blend in 2D geometry.

3.4.1 Cell viability and mitochondrial activity

Figure 10 shows fibroblasts (stained with Calcein AM) on Alg and Alg/E 2D hydrogels after 3, 7 and 10 days of incubation. To study the viability and morphology of living cells, calcein AM, which stains the cytoplasm of living cells, was used [70]. Calcein staining further gives information about the cell shape and membrane integrity, which are the hallmarks of the normal cell equilibrium. DAPI, a nucleic acid stain, was used to study the integrity of the nucleus [71]. In **Figure 10**, the progressive reduction in viable cell numbers on Alg hydrogel between day 3 and day 10 of culture is shown. On Alg hydrogels, the cells were found to be agglomerated, forming clusters after 10 days of culture, as also observed in our previous studies [18]. This indicates that on Alg hydrogel, cell-cell interactions are stronger than cell-material interactions resulting in a weakened attachment of cells to the material surface leading to clustering of cells. On Alg/E hydrogels, the number of cells was comparable at day 3. In contrast to pure Alg, the cells grown on Alg/E proliferated and retained their spread morphology over time. On day 7 and day 10, more viable cells with intact nuclei and cell membranes were found on Alg/E, as compared with Alg.

(**Figure 10**)

To confirm the microscopic observations, the metabolism of fibroblasts was determined by measuring their mitochondrial activity with WST-8 assay, as presented in **Figure 11**. Mitochondrial activity is an essential marker of normal cellular function, being affected by cell proliferation, apoptosis or cell death [72]. In metabolically active cells, tetrazolium compound is metabolized in the mitochondria and the product, formazan, is secreted into the medium, resulting in a change of color which is measured spectrophotometrically. The obtained results confirmed that on day 3, no major differences were detectable between fibroblasts grown on Alg and Alg/E. However, after 7 or 10 days of cultivation, the mitochondrial activity of fibroblasts grown on hybrid hydrogels was significantly higher, as compared to those grown on Alg. These results are in accordance with the above-presented microscopic observations of fibroblasts grown on different matrices.

(**Figure 11**)

4. Conclusions

Novel Alg/E hybrid hydrogel matrices (2D and 3D) were successfully produced using two different techniques, namely sonication and pressure-driven extrusion. The extensive physico-chemical characterization of the hydrogels demonstrated the positive effect of the presence of a native ECM protein, elastin, on the key properties of the alginate-based hydrogels. This study also highlights suitable cell-material interactions with primary fibroblasts, demonstrating the ability of 2D hybrid hydrogels to promote cell attachment, proliferation, spreading and viability. Our results indicate that the Alg/E hybrid hydrogel can be a promising biomaterial for soft-tissue regeneration and lay the foundation for future experiments to investigate the use of these hydrogels for engineering more complex scaffolds, for example by 3D printing approaches. Potential biomedical applications of Alg/E hybrid hydrogels will require further extensive analysis of cellular interactions with the 2D and 3D matrices.

Acknowledgements

This study was supported by the Emerging Fields project "TOPbiomat" of the University of Erlangen-Nuremberg (Germany) and in part by the German Science Foundation (DFG) (grant SI 2093/2-1 to R. Singh). The authors thank Dr. Menti Goudouri for FTIR measurements and Heike Kloos for help with cell culture experiments.

References

[1] Annabi N, Mithieux SM, Weiss AS, Dehghani F. Cross-linked open-pore elastic hydrogels based on tropoelastin, elastin and high pressure CO2. Biomaterials 2010;31:1655–65.

[2] Jia X, Kiick KL. Hybrid multicomponent hydrogels for tissue engineering. Macromol Biosci 2009;9:140–56.

[3] Lee KY, Mooney DJ. Hydrogels for Tissue Engineering. Chem Rev

2001;101:1869–80.

[4] Peppas N a. Hydrogels and drug delivery. Curr Opin Colloid Interface Sci 1997;2:531–7.

[5] Zagris N. Extracellular matrix in development of the early embryo. Micron 2001;32:427–38.

[6] Aumailley M, Gayraud B. Structure and biological activity of the extracellular matrix. J Mol Med (Berl) 1998;76:253–65.

[7] Gullberg D, Ekblom P. Extracellular matrix and its receptors during development. Int J Dev Biol 1995;39:845–54.

[8] Daley WP, Peters SB, Larsen M. Extracellular matrix dynamics in development and regenerative medicine. J Cell Sci 2008;121:255–64.

[9] Bosman FT, Stamenkovic I. Functional structure and composition of the extracellular matrix. J Pathol 2003;200:423–8.

[10] Karsdal M a, Nielsen MJ, Sand JM, Henriksen K, Genovese F, Bay-Jensen A-C, et al. Extracellular matrix remodeling: the common denominator in connective tissue diseases. Possibilities for evaluation and current understanding of the matrix as more than a passive architecture, but a key player in tissue failure. Assay Drug Dev Technol 2013;11:70–92.

[11] Varghese S, Elisseeff J. Hydrogels for musculoskeletal tissue engineering. Polym Regen Med 2006:95–144.

[12] Hamidi M, Azadi A, Rafiei P. Hydrogel nanoparticles in drug delivery. Adv Drug Deliv Rev 2008;60:1638–49.

[13] Gao C, Liu M, Chen J, Zhang X. Preparation and controlled degradation of oxidized sodium alginate hydrogel. Polym Degrad Stab 2009;94:1405–10.

[14] Wang L, Shansky J. Design and fabrication of a biodegradable, covalently crosslinked shape-memory alginate scaffold for cell and growth factor delivery. Tissue Eng Part A 2012;18:2000–7.

[15] Leal-Egaña A, Braumann U-D, Díaz-Cuenca A, Nowicki M, Bader A. Determination of pore size distribution at the cell-hydrogel interface. J Nanobiotechnology 2011;9:24.

[16] Balakrishnan B, Mohanty M, Umashankar PR, Jayakrishnan a. Evaluation of an in situ forming hydrogel wound dressing based on oxidized alginate and gelatin. Biomaterials 2005;26:6335–42.

[17] Melchels FPW, Domingos M a. N, Klein TJ, Malda J, Bartolo PJ, Hutmacher DW. Additive manufacturing of tissues and organs. Prog Polym Sci 2012;37:1079–104.

[18] Sarker B, Papageorgiou DG, Silva R, Tobias Zehnder, Gul-E-Noor F, Bertmer M, et al. Fabrication of alginate – gelatin crosslinked hydrogel microcapsules and evaluation of the microstructure and physico-chemical properties. J. Mater. Chem. B, 2014; 2: 1470-1482.

[19] Annabi N, Mithieux SM, Camci-Unal G, Dokmeci MR, Weiss AS, Khademhosseini A. Elastomeric Recombinant Protein-based

Biomaterials. Biochem Eng J 2013;77:110–8.

[20] Sandberg L, Soskel N, Leslie J. Elastin structure, biosynthesis, and relation to disease states. N Engl J Med 1981:1–4.

[21] Nettles DL, Chilkoti A, Setton L a. Applications of elastin-like polypeptides in tissue engineering. Adv Drug Deliv Rev 2010;62:1479–85.

[22] Madsen K, Moskalewski S, von der Mark K, Friberg U. Synthesis of proteoglycans, collagen, and elastin by cultures of rabbit auricular chondrocytes--relation to age of the donor. Dev Biol 1983;96:63–73.

[23] Mecham R, Heuser J. The elastic fiber. Cell Biol Extracell Matrix 1991:366–81.

[24] Long J, Tranquillo R. Elastic fiber production in cardiovascular tissue-equivalents. Matrix Biol 2003;22:339–50.

[25] Daamen W, Veerkamp J. Elastin as a biomaterial for tissue engineering. 2007.

[26] Foster J a, Bruenger E, Gray WR, Sandberg LB. Isolation and amino acid sequences of tropoelastin peptides. J Biol Chem 1973;248:2876–9.

[27] Cox B, Starcher B, Urry D. Coacervation of α-elastin results in fiber formation. Biochim Biophys Acta 1973;317:209–13.

[28] Kaibara K, Sakai K, Okamoto K, Uemura Y, Miyakawa K, Kondo M. Alpha-elastin coacervate as a protein liquid membrane: effect of pH on transmembrane potential responses. Biopolymers 1992;32:1173–80.

[29] Annabi N, Mithieux SM, Weiss AS, Dehghani F. The fabrication of elastin-based hydrogels using high pressure CO(2). Biomaterials 2009;30:1–7.

[30] Leach JB, Wolinsky JB, Stone PJ, Wong JY. Crosslinked alpha-elastin biomaterials: towards a processable elastin mimetic scaffold. Acta Biomater 2005;1:155–64.

[31] Girotti A, Reguera J, Rodríguez-Cabello JC, Arias FJ, Alonso M, Matestera A. Design and bioproduction of a recombinant multi(bio)functional elastin-like protein polymer containing cell adhesion sequences for tissue engineering purposes. J Mater Sci Mater Med 2004;15:479–84.

[32] Koria P, Yagi H, Kitagawa Y, Megeed Z, Nahmias Y, Sheridan R, et al. Self-assembling elastin-like peptides growth factor chimeric nanoparticles for the treatment of chronic wounds. Proc Natl Acad Sci U S A 2011;108:1034–9.

[33] Trabbic-Carlson K, Setton L a, Chilkoti A. Swelling and mechanical behaviors of chemically cross-linked hydrogels of elastin-like polypeptides. Biomacromolecules 2003;4:572–80.

[34] Silva R, Ferreira H, Little C, Cavaco-Paulo A. Effect of ultrasound parameters for unilamellar liposome preparation. Ultrason Sonochem 2010;17:628–32.

[35] Lowry OC, Rosebrough N. Protein measurement with the Folin phenol reagent. J Biol Chem 1951;193:265–75.

[36] Peppas NA, Bures P, Leobandung W, Ichikawa H. Hydrogels in pharmaceutical formulations. Eur J Pharm Biopharm 2000;50:27–46.

[37] Ming J, Zuo B. A novel silk fibroin/sodium alginate hybrid scaffolds. Polym Eng Sci 2013:1–8.

[38] Debelle L, Alix a. JP, Jacob M-P, Huvenne J-P, Berjot M, Sombret B, et al. Bovine Elastin and -Elastin Secondary Structure Determination by Optical Spectroscopies. J Biol Chem 1995;270:26099–103.

[39] Haris PI, Severcan F. FTIR spectroscopic characterization of protein structure in aqueous and non-aqueous media. J Mol Catal B Enzym 1999;7:207–21.

[40] Chittur KK. FTIR/ATR for protein adsorption to biomaterial surfaces. Biomaterials 1998;19:357–69.

[41] Dong a, Huang P, Caughey WS. Protein secondary structures in water from second-derivative amide I infrared spectra. Biochemistry 1990;29:3303–8.

[42] Dong A, Huang P, Caughey WS. Protein secondary structures in water from second-derivative amide I infrared spectra. Biochemistry 1990;29:3303–8.

[43] Byler DM, Susi H. Examination of the secondary structure of proteins by deconvolved FTIR spectra. Biopolymers 1986;25:469–87.

[44] Hu X, Kaplan D, Cebe P. Dynamic Protein - Water Relationships during - Sheet Formation. Macromolecules 2008;41:3939–48.

[45] Hu X, Kaplan D, Cebe P. Determining Beta-Sheet Crystallinity in Fibrous Proteins by Thermal Analysis and Infrared Spectroscopy. Macromolecules 2006;39:6161–70.

[46] Wang X, Kluge J a, Leisk GG, Kaplan DL. Sonication-induced gelation of silk fibroin for cell encapsulation. Biomaterials 2008;29:1054–64.

[47] Yucel T, Cebe P, Kaplan DL. Vortex-induced injectable silk fibroin hydrogels. Biophys J 2009;97:2044–50.

[48] Samal SK, Kaplan DL, Chiellini E. Ultrasound Sonication Effects on Silk Fibroin Protein. Macromol Mater Eng 2013;298:1201–8.

[49] Mason TJ. Sonochemistry and the environment - providing a “green” link between chemistry, physics and engineering. Ultrason Sonochem 2007;14:476–83.

[50] Paulusse JOSMJ, Sijbesma RP. Ultrasound in Polymer Chemistry : Revival of an Established Technique. J Polym Sci Apolym Chem 2006;44:5445–53.

[51] Rae J, Ashokkumar M, Eulaerts O, von Sonntag C, Reisse J, Grieser F. Estimation of ultrasound induced cavitation bubble temperatures in aqueous solutions. Ultrason Sonochem 2005;12:325–9.

[52] Bang JH, Suslick KS. Applications of Ultrasound to the Synthesis of Nanostructured Materials. Adv Mater 2010;22:1039–59.

[53] Suslick KS, Grinstaff MW. Protein microencapsulation of nonaqueous liquids. J Am Chem Soc 1990;112:7807–9.

[54] Suslick S, Fang M. Acoustic cavitation and its 1999:335–53.

[55] Soares JP, Santos JE, Chierice GO, Cavalheiro ETG. Thermal behavior of alginic acid and its sodium salt. Eclet Quim 2004;29:57–63.

[56] Gaharwar AK, Peppas NA, Khademhosseini A. Nanocomposite hydrogels for biomedical applications. Biotechnol Bioeng 2013;9999:1–12.

[57] Xiao W, Liu W, Sun J, Dan X, Wei D, Fan H. Ultrasonication and Genipin Cross-Linking to Prepare Novel Silk Fibroin-Gelatin Composite Hydrogel. J Bioact Compat Polym 2012;27:327–41.

[58] Tham WL, Chow WS, Mohad Ishak ZA. Simulated body fluid and water absorption effects on poly(methyl methacrylate)/hydroxyapatite denture base composites. eXPRESS Polym Lett 2010;4:517–28.

[59] Zhou C, Ma H. Ultrasonic Degradation of Polysaccharide from a Red Algae (Porphyra yezoensis) AND. J Agric Food Chem 2006;54:2223–8.

[60] Ferrero C, Massuelle D, Doelker E. Towards elucidation of the drug release mechanism from compressed hydrophilic matrices made of cellulose ethers. II. Evaluation of a possible swelling-controlled drug release mechanism using dimensionless analysis. J Control Release 2010;141:223–33.

[61] Silva, R., et al., Hybrid hydrogels based on keratin and alginate for tissue engineering. J. Mater. Chem. B, 2014; 2: 5441-5451.

[62] Sobral JM, Caridade SG, Sousa RA, Mano JF, Reis RL. Three-dimensional plotted scaffolds with controlled pore size gradients : Effect of scaffold geometry on mechanical performance and cell seeding efficiency. Acta Biomater 2011;7:1009–18.

[63] Silva JM, Georgi N, Costa R, Sher P, Reis RL, Van CA. Nanostructured 3D Constructs Based on Chitosan and Chondroitin Sulphate Multilayers for Cartilage Tissue Engineering. PLoS One 2013;8:1–11.

[64] Caridade S, Merino E, Alves NM, de Zea Bermudez V, Boccaccini AR, Mano JF. Chitosan membranes containing micro or nano-size bioactive glass particles: evolution of biomineralization followed by in-situ dynamic mechanical analysis. J Mech Behav Biomed Mater 2012;20:173–83.

[65] Sachlos E, Czernuszka JT. Making tissue engineering scaffolds work. Review: the application of solid freeform fabrication technology to the production of tissue engineering scaffolds. Eur Cell Mater 2003;5:29–39; discussion 39–40.

[66] Wang Y, Ren J, Xia K, Wang S, Yin T, Xie D, et al. Effect of mitomycin on normal dermal fibroblast and HaCat cell: an in vitro study. J Zhejiang Univ Sci B 2012;13:997–1005.

[67] Varga J, Rosenbloom J, Jimenez S a. Transforming growth factor beta (TGF beta) causes a persistent increase in steady-state amounts of type I and type III collagen and fibronectin mRNAs in normal human dermal fibroblasts. Biochem J 1987;247:597–604.

[68] Roberts a B, Sporn MB, Assoian RK, Smith JM, Roche NS, Wakefield LM, et al. Transforming growth factor type beta: rapid induction of fibrosis

and angiogenesis in vivo and stimulation of collagen formation in vitro. Proc Natl Acad Sci U S A 1986;83:4167–71.

[69] Stevenson S, Nelson LD, Sharpe DT, Thornton MJ. 17beta-estradiol regulates the secretion of TGF-beta by cultured human dermal fibroblasts. J Biomater Sci Polym Ed 2008;19:1097–109.

[70] Joshi C, Karumuri B, Newman JJ, Decoster MA. Cell morphological changes combined with biochemical assays for assessment of apoptosis and apoptosis reversal . Curr Microsc Contrib to Adv Sci Technol (A Méndez-Vilas, Ed) 2012:756–62.

[71] Ioannou YA, Chen FW. Quantitation of DNA fragmentation in apoptosis. Nucleic Acids Res 1996;24:992–3.

[72] Wen Y, Wang H, Kho S, Rinkiko S, Sheng X, Shen H, et al. Hydrogen Sulfide Protects HUVECs against Hydrogen Peroxide Induced Mitochondrial Dysfunction and Oxidative Stress. PLoS One 2013;8:1–10.

Figures

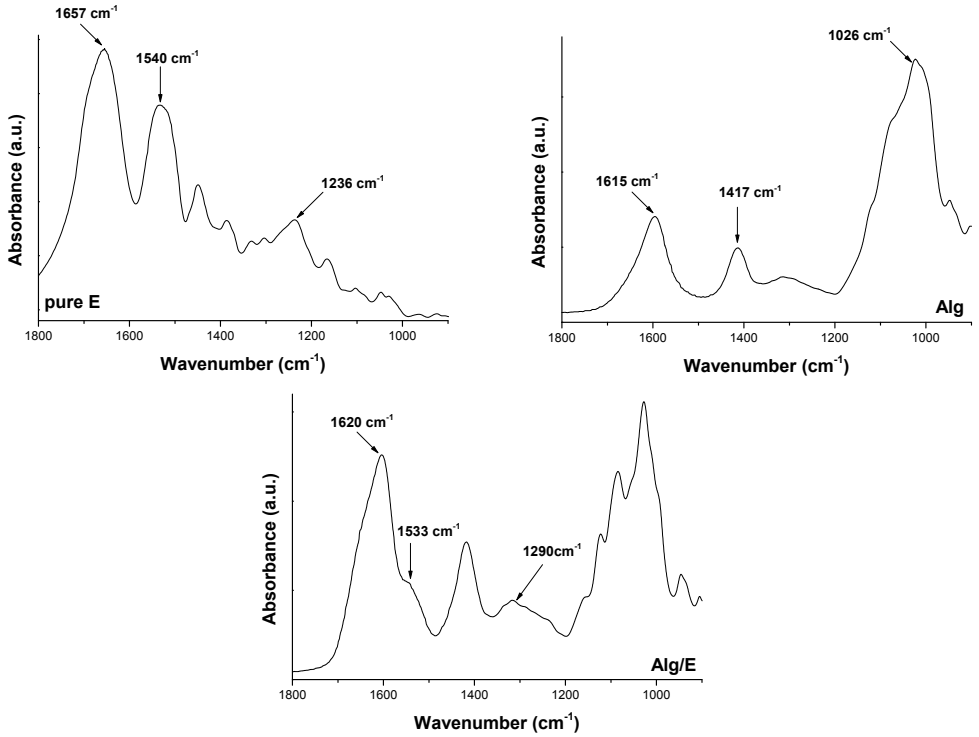

Figure 1: FTIR spectra intervals (1800-900 cm^{-1}) of pure elastin and 2D hydrogels of Alg and Alg/E.

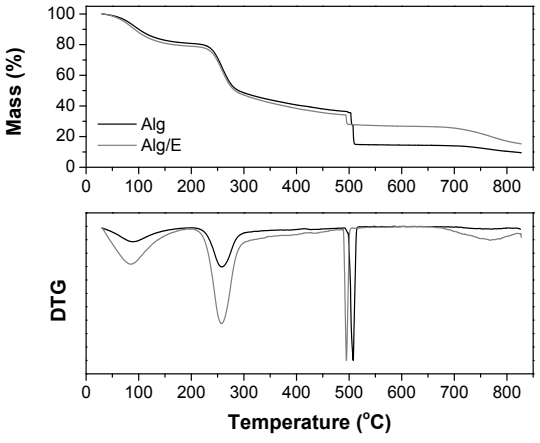

a)

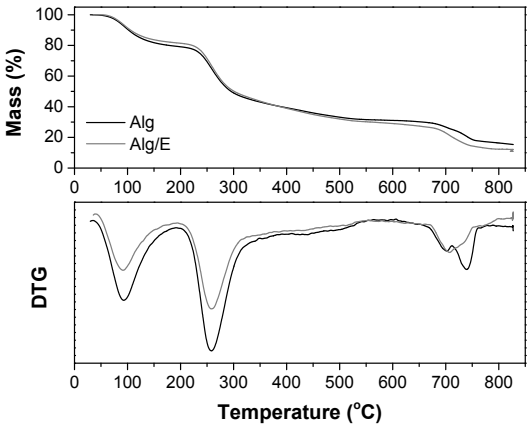

b)

Figure 2: Mass loss (%) and derivative thermogravimetric analysis (DTG) curves of 2D (a) and 3D hydrogels (b) obtained from Alg, and Alg/E.

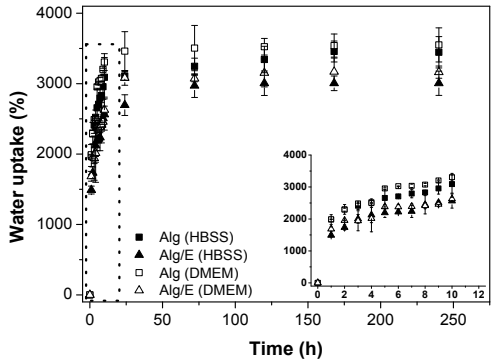

a)

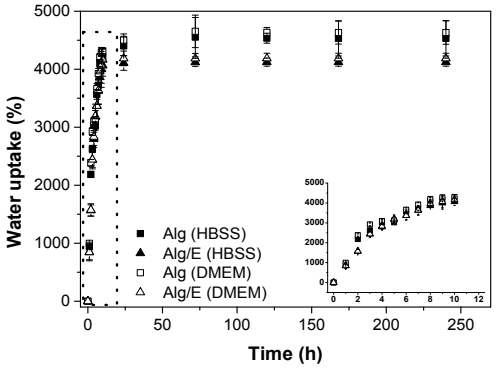

b)

Figure 3: Water uptake studies of hydrogels in two different media (DMEM and HBSS): a) 2D hybrid hydrogels and b) 3D hybrid hydrogels.

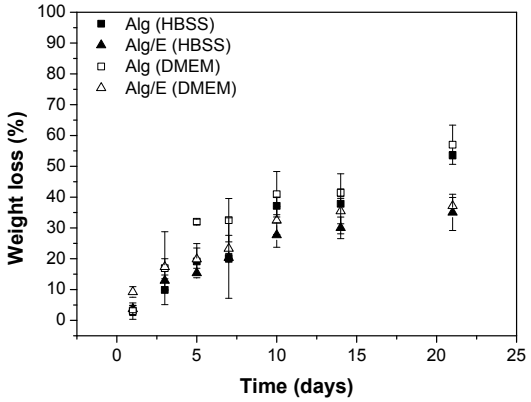

Figure 4: Weight loss measurements of 2D hydrogels after 21 days of incubation in HBSS and DMEM.

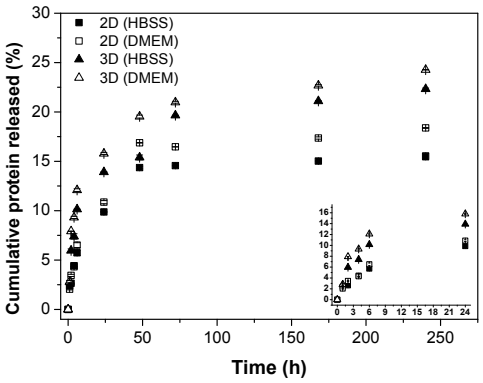

Figure 5: Cumulative elastin released (%) as a function of incubation time in HBSS and in DMEM for the different geometries of hydrogels: 2D and 3D.

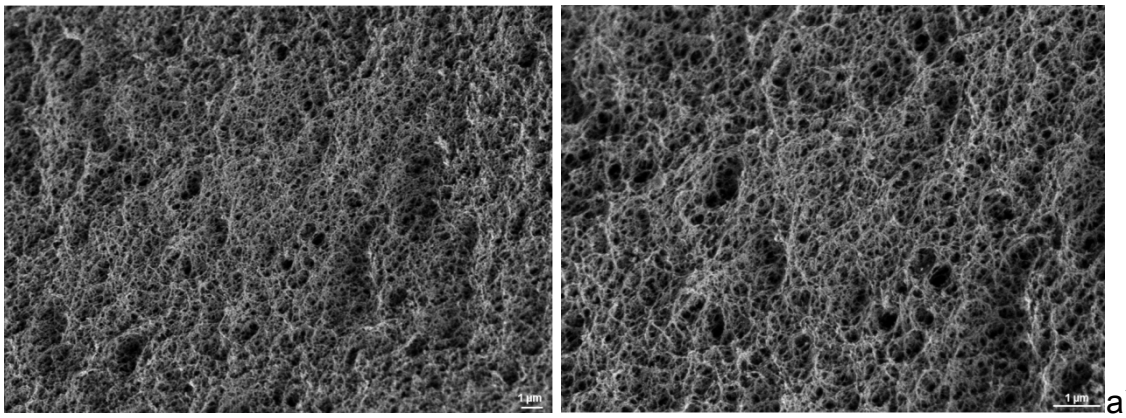

a)

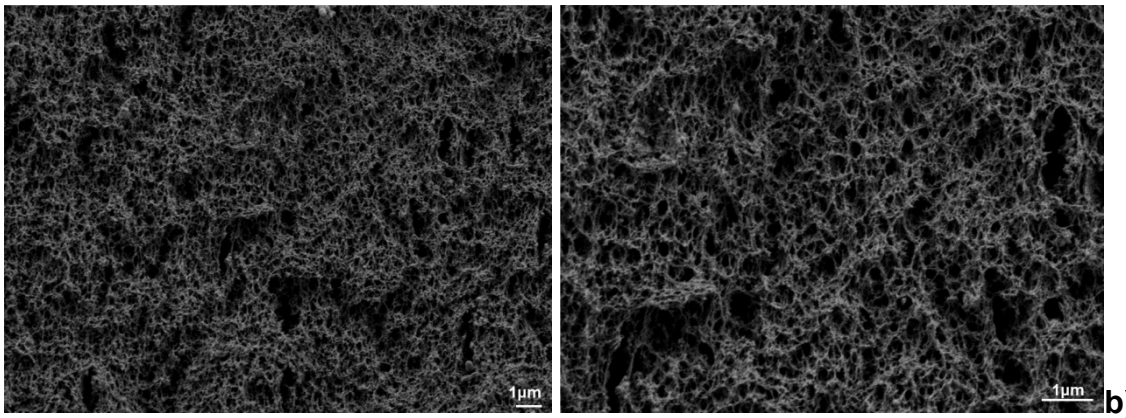

Figure 6: SEM cross-section images of Alg (a) and Alg/E (b) 2D hydrogels showing similar porosity. (Fig (a) reproduced from ref. [61], with permission of Royal Soc. of Chemistry).

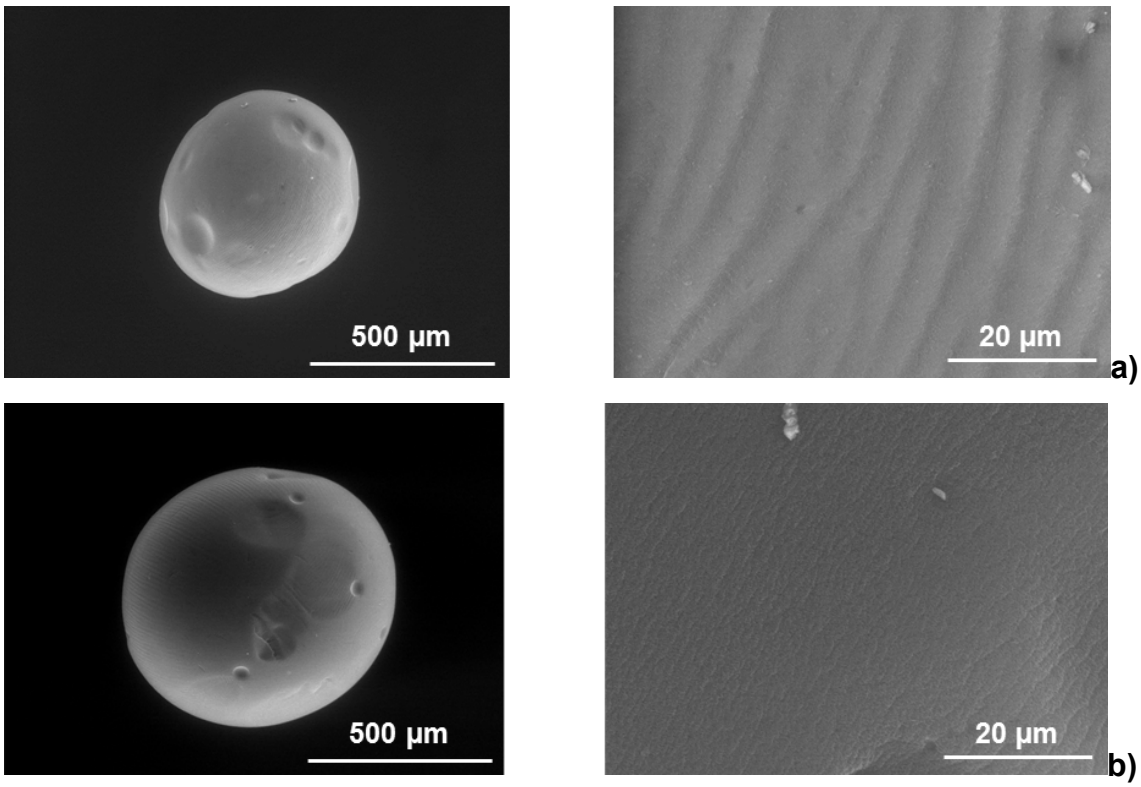

Figure 7: SEM images of 3D hydrogels showing complete microcapsule and their surfaces: Alg (a) and Alg/E (b). (Fig (a) reproduced from ref. [61], with permission of Royal Soc. of Chemistry).

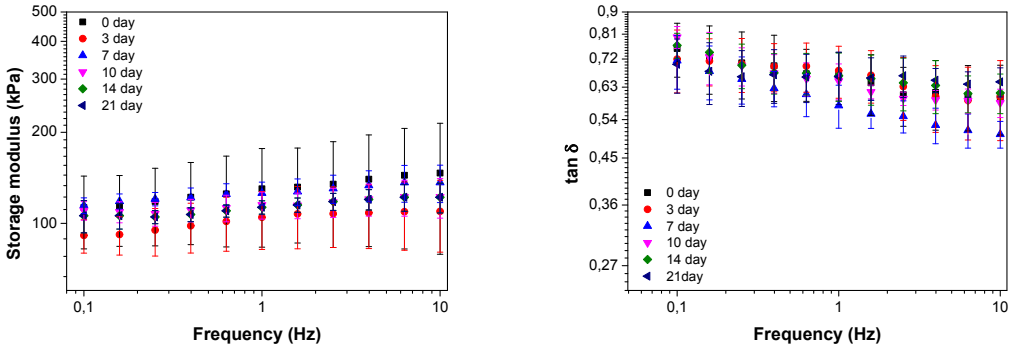

a)

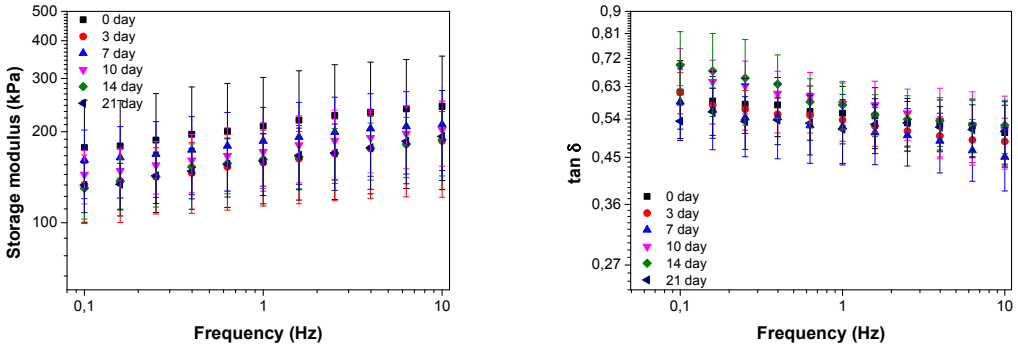

b)

Figure 8: DMTA scans of (a) Alg; and (b) Alg/E hydrogels immediately after preparation and after 21 days of incubation in DMEM.

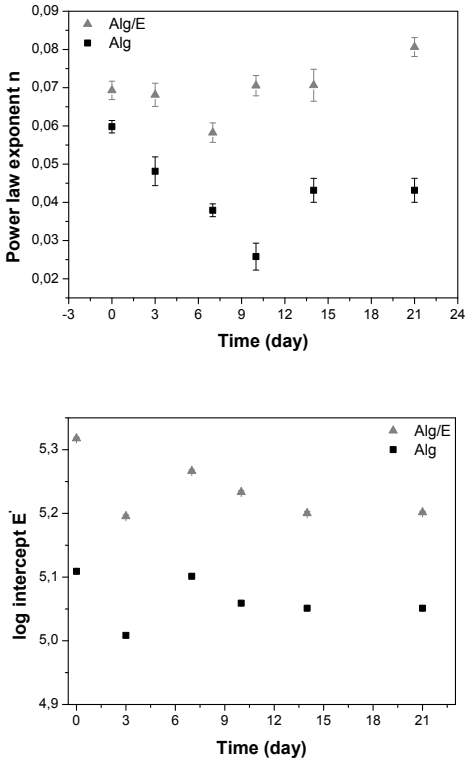

Figure 9: Power law exponent n (a) and log intercept E' of the fitting curves of storage moduli over 21 days.

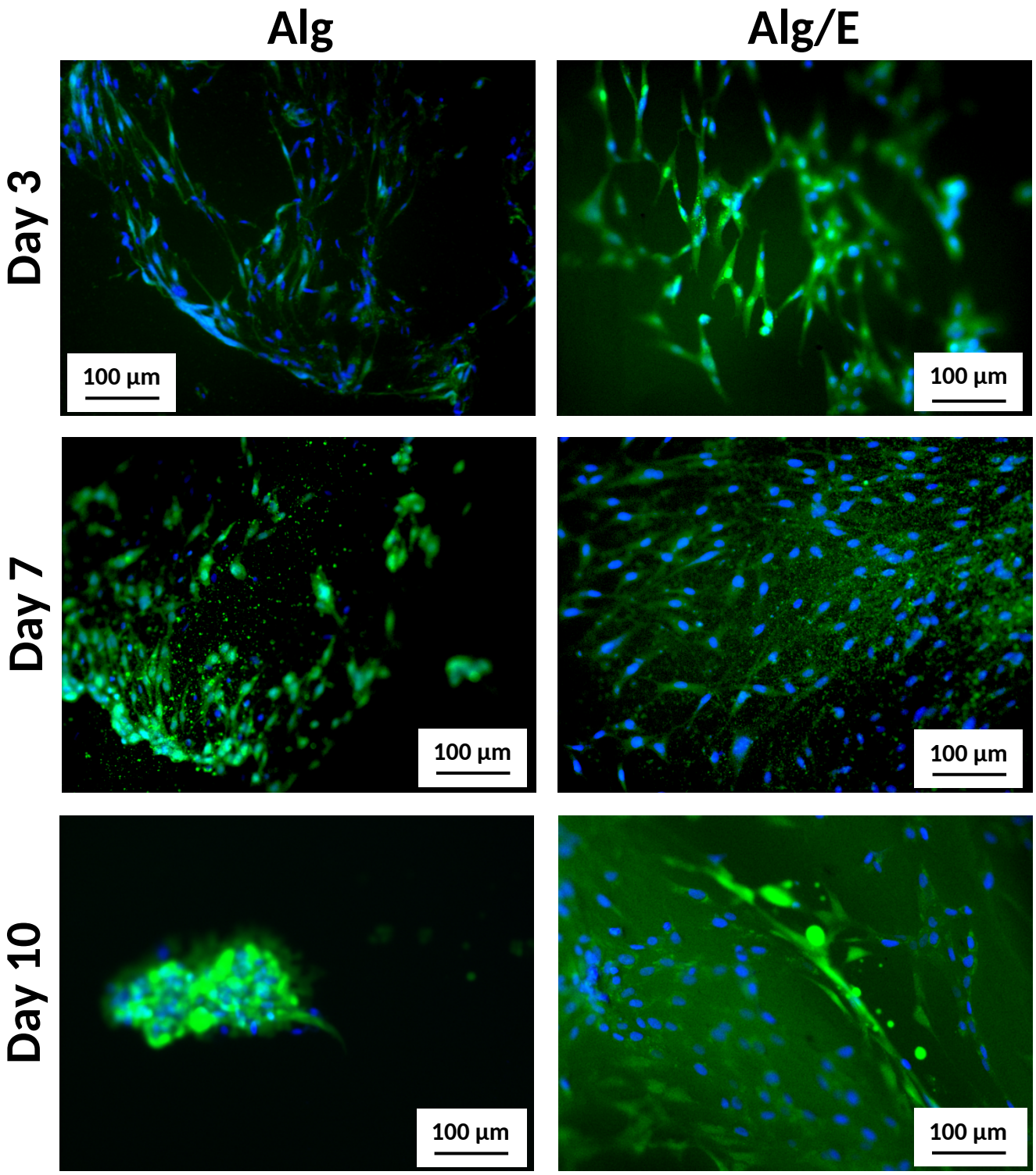

Figure 10: Fluorescent staining with Calcein/DAPI of fibroblasts on 2D hydrogels after 3, 7 and 10 days. The cells were stained with Calcein to detect living cells (green) and DAPI to detect nuclei (blue).

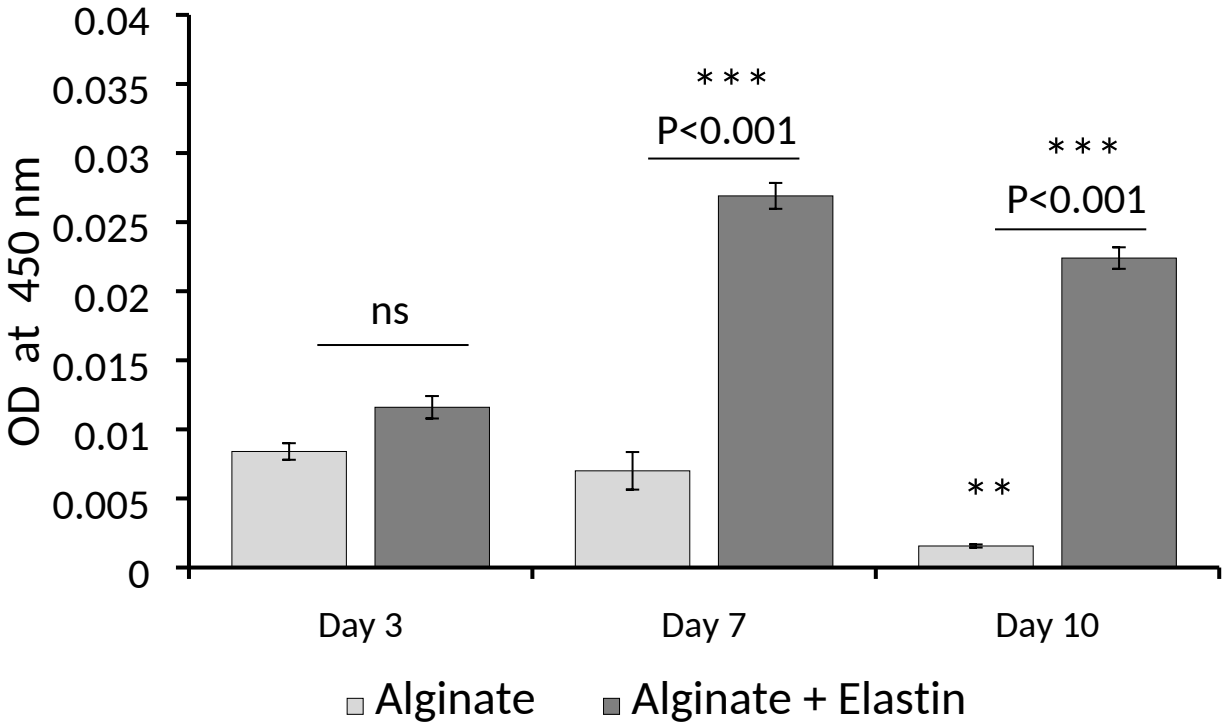

Figure 11: Mitochondrial activity of fibroblasts on 2D hydrogels after 3, 7 and 10 days of culture. Data are expressed as mean SEM of 3 independent experiments. Statistically significant differences between the Alg and Alg/E samples on the respective days are as indicated; ns, not significant. Statistically significant differences between cells grown on respective hydrogel types are indicated with symbols: ***p< 0.001; ** p< 0.01 versus respective hydrogel type on day 3.

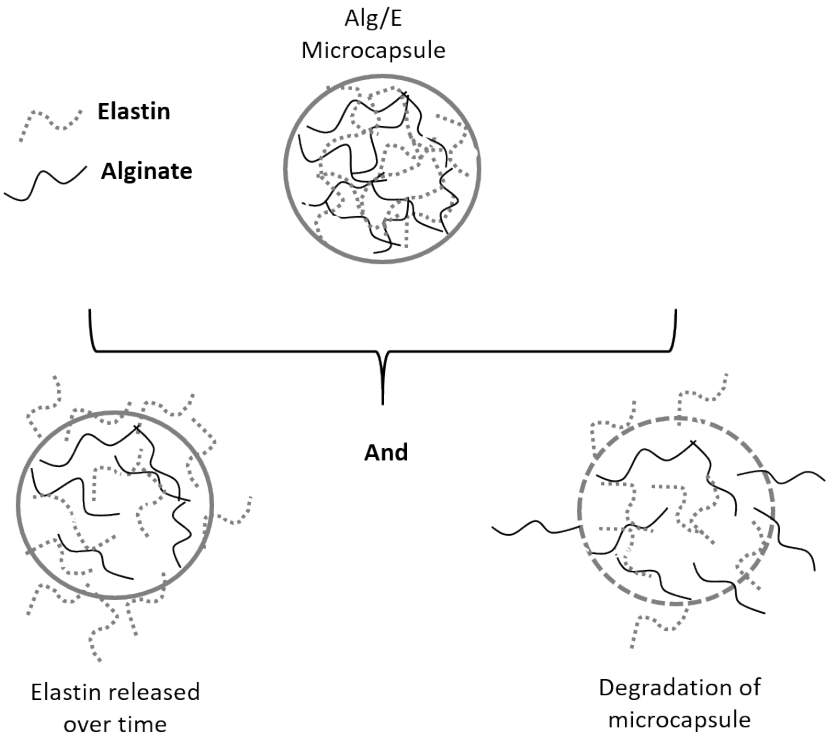
Alg/E
Microcapsule
Elastin
Alginate
And
Elastin released
over time
Degradation of
microcapsule

Table 1: Model compound release kinetic parameters obtained from fitting the experimental release data to Eq. (5)

Sample		Kinetic parameters		
		n	k	R^2
2D	HBSS	0.533	0.318	0.9835
	DMEM	0.521	0.348	0.9863
3D	HBSS	0.299	0.701	0.9916
	DMEM	0.258	0.835	0.9861